*Int. J. Electrochem. Sci.*, 15 **(2020)** 3068 – 3088, doi: 10.20964/2020.04.55

International Journal of
ELECTROCHEMICAL
SCIENCE
www.electrochemsci.org

# Thermodynamic Analyses of a Phosphoric Acid Fuel Cell / Thermoelectric Generator Hybrid System with the Thomson Effect

*Jing Zhang*[1], *Xinru Guo*[1], *Yanhong Guo*[1], *Houcheng Zhang*[1,*], *Shujin Hou*[2,*], *Yanting Tian*[3]

[1] Department of Microelectronic Science and Engineering, Ningbo University, Ningbo 315211, China
[2] College of Physics and Electronic Engineering, Nanyang Normal University, Nanyang 473061, China
[3] College of Physics and Optoelectronics, Taiyuan University of Technology, Taiyuan 030024, China
[*]E-mail: zhanghoucheng@nbu.edu.cn (H. Zhang); houshujingrb@163.com (S. Hou).

*Received:* 8 December 2019 / *Accepted:* 5 February 2020 / *Published:* 10 March 2020

Apart from producing electricity, phosphoric acid fuel cell (PAFC) releases a lot of exhaust heat during operation. A hybrid system incorporating a PAFC, a regenerator and a thermoelectric generator (TEG) is presented to recover the exhaust heat from the PAFC via TEG. Not only the Peltier and Seebeck effects but also the Thomson effect are taken into account to accurately describe the TEG model. The energetic and exergetic performances for the PAFC-TEG hybrid system are studied using thermodynamic criteria, including output power, energetic efficiency, exergy destruction rate and exergetic efficiency. The relationships between the PAFC operating current density and the TEG current density at different temperatures are derived. The maximum power density of the hybrid system and its corresponding energetic efficiency and exergetic efficiency are 6.6%, 7.8% and 7.7% higher than that of the single PAFC system, respectively. Meanwhile, the corresponding exergy destruction rate density is found to be decreased by 7.8%. The optimum operating ranges of these four vital performance parameters for the PAFC-TEG system are obtained by taking the maximum power output as the optimization criterion. The influences of Thomson effect on the PAFC-TEG system thermodynamic performance are also discussed. Furthermore, the effects of the operating conditions and designing parameters on the PAFC-TEG system performance are investigated through exhaustive parametric studies.

**Keywords**: Phosphoric acid fuel cell; Exergy analysis; Energy analysis; Thermoelectric generator; Thomson effect

## 1. INTRODUCTION

The shortage of fossil fuels and serious environment pollution have seriously hindered the global economic and social development. Thus, it is urgent to develop renewable and sustainable energies to alleviate the problems. A fuel cell, a kind of energy conversion device that converts chemical energy directly into electricity [1], is a more suitable renewable system than wind and solar energy systems due to its lower emission and high energy efficiency [2]. According to the electrolyte types, fuel cells can be classified into molten carbonate fuel cells (MCFCs) [3, 4], phosphoric acid fuel cells (PAFCs) [5, 6], alkaline fuel cells (AFCs) [7-9], proton exchange membrane fuel cells (PEMFCs) [10-12] and solid oxide fuel cells (SOFCs) [13, 14]. Amongst, PAFCs are the most widely used and closest to commercialization due to their high durability, low working temperature and low cost [15].

In the last decade, a great quantity of theoretical and experimental studies have been done on the PAFC performance improvement, including transport phenomena and electrochemical processes [16, 17], materials fabrication [18, 19] and performance optimization at hsystem level [20, 21] and so on [22, 23]. In addition, extensive studies used kinds of bottoming cycles to recover the waste heat of PAFC to achieve a higher fuel utilization rate [24-27]. So far, various devices have been presented as bottoming cycles for PAFCs, including refrigeration cycle [24], thermally regenerative electrochemical cycle [25] and thermoelectric generator (TEG) [26, 27].

TEGs are solid-state energy converters that can directly transform heat into electricity via the Seebeck effect [28, 29]. TEGs are environmental-friendly, highly reliable and durable because they can work without rotating or sliding assemblies [30]. In addition to stationary power generators, TEGs are also attractive as portable devices because of their compactness and high output power [31, 32]. TEGs are receiving more and more attention in scientific community, especially in the area of low-level waste heat recovery.

In recent years, many innovative systems have been proposed in recycling the waste heat from fuel cell using TEGs [26, 27, 33-40]. Among them, Chen et al. [26] coupled a TEG subsystem to recycle the PAFC waste heat, and they concluded that the maximum output power density for the hybrid system was 150 W $m^{-2}$ higher than that for the single PAFC system. In addition, Açıkkalp et al. [27] evaluated a PAFC-TEG hybrid system with economic and thermoeconomic viewpoints. Gao et al. [34] used an optimized TEG subsystem to recover the exhaust heat from a high-temperature PEMFC stack. However, the influences of the Thomson effect on the TEG had been neglected in these studies.

The Thomson effect has an unnegligible influence on the TEG performance, and scientists have widely studied this topic [41-46]. For example, Chen et al. [41] discussed the impacts of the Thomson effect on a TEG under different operating conditions. Kaushik et al. [45] and Lamba et al. [46] carried out the energetic and exergetic analyses of a TEG considering the Thomson effect and found that the Thomson effect deteriorated the energetic and exergetic performances of the TEG. Manikandan et al. [47] investigated the influences of Thomson effect on the performance of a two-stage TEG, and they found that the optimum number of thermocouples for the two-stage TEG was different from that of previous studies due to the inclusion of Thomson effect. Thus, it is meaningful to study the Thomson effect on the PAFC-TEG hybrid system.

In this article, a hybrid system model composed of a PAFC, a regenerator and a TEG with Thomson effect will be put forward, in which the TEG further recovers the waste heat from PAFC into electricity. The proposed hybrid system model will be mathematically described by considering various irreversible losses within the system. The mathematical relationship between the PAFC working current density and the TEG electric current will be derived. The proposed system will be compared with the single PAFC system to verify the effectiveness of the proposed hybrid system. In addition, the influences of Thomson effect on the PAFC-TEG system performance will be also revealed. At last, the influences of some vital designing parameters and operating conditions on the hybrid system performance will be discussed through extensive parametric studies.

## 2. SYSTEM DESCRIPTION

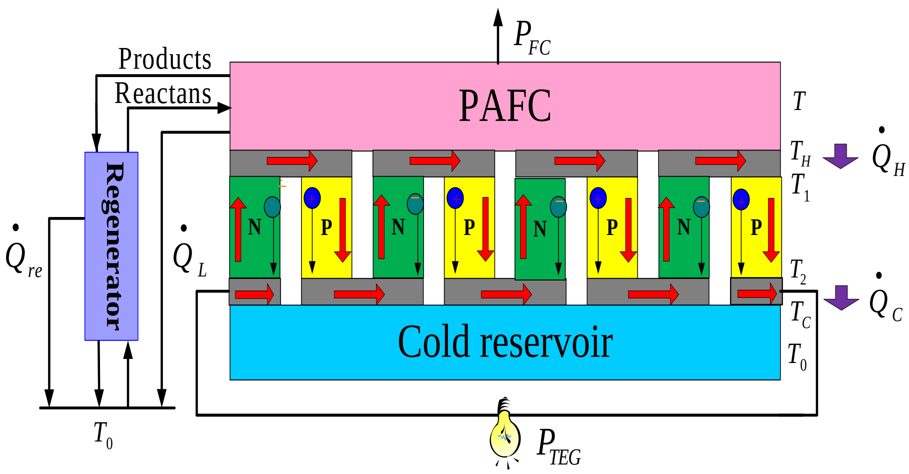


**Figure 1.** Schematic diagram of the PAFC-TEG hybrid system.

As shown in Fig. 1, the PAFC operating at temperature $T$ directly transforms the chemical energy contained in hydrogen and oxygen into electric power $P_{FC}$ and exhaust heat. A portion of the exhaust heat, $\dot{Q}_L$, is inevitably diffused into the surroundings at temperature $T_0$ via conduction or convection heat transfer. Another portion of the waste heat, $\dot{Q}_{re}$, is transferred to the regenerator for compensating the regenerative loss. The rest of the waste heat, $\dot{Q}_H$, will be converted into electrical power $P_{TEG}$ via the TEG. Then the waste heat released by the TEG, $\dot{Q}_C$, will be dissipated into the surroundings. $T_1$ and $T_2$ are, respectively, the TEG hot junction and cold junction temperatures, and $T_H$ and $T_C$ are the TEG hot side and cold side temperatures, respectively.

In the subsequent analyses, the assumptions are given as follows [45, 47-49]:

- Reactants ($H_2$ and $O_2$) of the PAFC are consumed completely;
- The amount of $H_2$ and $O_2$ are fed according to the operating current density of PAFC;
- Variations of kinetic and potential energies are ignored;
- All heat-transfer processes obey the Newton's law;
- Both PAFC and TEG are worked under steady conditions;
- TEG is exoreversible;
- The electrical resistance and thermal conductance for the conducting metals of TEG are

ignored;

- The contact electrical resistance between hot and cold junctions equals 10% of the total TEG resistance;
- The thermal resistance between the TEG junctions is neglected.

### *2.1. PAFC*

The PAFC is mainly composed of a positive electrode and a negative electrode and an electrolyte with the concentrated phosphoric acid solution. The overall electrochemical reaction in PAFC is: $H_2(g)+1/2O_2(g) \rightarrow H_2O(g)+\text{electricity}+\text{heat}$. The irreversible losses in PAFC are mainly caused by activation overpotential ($U_{act}$), ohmic overpotential ($U_{ohm}$) and concentration overpotential ($U_{con}$). Considering these irreversible losses, the output voltage of a PAFC can be calculated based on the information in Table 1 and Table 2.

**Table 1.** Thermodynamic parameters of $H_2$, $O_2$ and $H_2O$, where (g) and (l) stand for gas and liquid phases, respectively [25].

| Compound (-) | $\Delta g^0$ (J mol$^{-1}$) | $\Delta h^0$ (J mol$^{-1}$) | $\Delta s^0$ (J mol$^{-1}$) |
|---|---|---|---|
| $H_2$ (g) | 0 | 0 | 131 |
| $O_2$ (g) | 0 | 0 | 205 |
| $H_2O$ (g) | - | - | - |
| $H_2O$ (l) | 237,200 | 285,800 | 70 |

The output power $P_{FC}$ and energetic efficiency $\eta_{FC}$ of the PAFC are, respectively, given by [50, 51]

$$P_{FC} = jAU \tag{1}$$

and

$$\eta_{FC} = \frac{P_{FC}}{-\Delta \dot{H}} \tag{2}$$

where $j$ is the PAFC operating current density; $A$ is the PAFC effective polar plate area; $-\Delta \dot{H} = -\frac{jA\Delta h}{n_e F}$ is the overall energy generated of the PAFC per unit time; $\Delta h$ stands for the electrochemical reaction molar enthalpy change; and $n_e$ stands for the number of electrons involved for each hydrogen molecule.

Thus, the exergy destruction rate of PAFC, $ExD_{FC}$, can be defined as [47]

$$ExD_{FC} = -\Delta\dot{G} - T\Delta\dot{S}\left(1-\frac{T_0}{T}\right) - P_{FC} \quad (3)$$

where $-\Delta\dot{G} = -\frac{jA\Delta g}{n_e F}$ is the total Gibbs free energy change rate [47], and $\Delta g$ is the molar Gibbs free energy change. $-\Delta\dot{S} = -\frac{jA\Delta s}{n_e F}$ is the total entropy change rate [47], and $\Delta s$ is the molar entropy change.

The exergetic efficiency of PAFC, $\varphi_{FC}$, can be given by [47]

$$\varphi_{FC} = \frac{P_{FC}}{-\Delta\dot{G} - T\Delta\dot{S}\left(1-\frac{T_0}{T}\right)} \quad (4)$$

*2.2. Regenerator*

It is often assumed that the regenerative loss rate $\dot{Q}_{re}$ in the regenerator varies with temperature difference between the inlet reactants and the exhaust products [48], i.e.,

$$\dot{Q}_{re} = K_{re}A_{re}(1-\varepsilon)\left(T-T_0\right) \quad (5)$$

where $K_{re}$ stands for the regenerator heat-transfer coefficient; $A_{re}$ stands for the regenerator heat-transfer area, and $\varepsilon$ is the regenerator effectiveness.

*2.3. TEG*

The TEG works between the PAFC (hot reservoir) and the environment (cold reservoir), as shown in Fig. 1. The thermocouple number of the TEG is $n$, and each thermocouple is composed of three metal connectors, two ceramic plates, a P-type semiconductor leg and an N-type semiconductor leg [52]. In this work, the thermoelectric material is Bismuth Telluride ($Bi_2Te_3$), and its Seebeck coefficient $\alpha$, electrical resistivity $\kappa$ and thermal conductivity $\rho$ are, respectively, given by [53]

$$\alpha = \alpha_P - \left(-\alpha_N\right) = 2\times\left(22224.0 + 930.6T_{avg} - 0.9905T_{avg}^2\right)\times 10^{-9} \quad (6)$$

$$\kappa_P = \kappa_N = \left(62605.0 - 277.7T_{avg} + 0.4131T_{avg}{}^2\right)\times 10^{-4} \quad (7)$$

and

$$\rho_P = \rho_N = \left(5112.0 + 163.4T_{avg} + 0.6279T_{avg}{}^2\right)\times 10^{-10} \quad (8)$$

where $T_{avg} = 0.5\left(T_H + T_C\right)$; and $P$ and $N$ stand for the P-type and N-type semiconductor materials, respectively.

The Thomson coefficient $\tau$ is defined as [54]

$$\tau = T\frac{\partial\alpha}{\partial T} \quad (9)$$

From Eqs. (6) and (9), $\tau$ can be further rewritten as [55]

$$\tau = 2\times\left(930.6T_{avg} - 1.981T_{avg}^2\right)\times 10^{-9} \quad (10)$$

Taking the Thomson, Seebeck and Peltier effects into account, the energy balance equations at the TEG sides can be, respectively, expressed as [56]

$$\dot{Q}_H = n\left[\alpha_1 I T_1 - \frac{I^2 R_g}{2} + K\left(T_1 - T_2\right) - \frac{\tau_1 I (T_1 - T_2)}{2}\right] \tag{11}$$

and

$$\dot{Q}_C = n\left[\alpha_2 I T_2 + \frac{I^2 R_g}{2} + K\left(T_1 - T_2\right) + \frac{\tau_2 I (T_1 - T_2)}{2}\right] \tag{12}$$

where $\alpha_i$ and $\tau_i$ are Seebeck coefficient and Thomson coefficient at temperature $T_i$ ( $i = 1, 2$ ), respectively.

The electrical resistance $R_g$ and thermal conductance $K$ of a thermocouple can be, respectively, expressed as [57]

$$R_g = \left(\frac{\rho_P L_P}{S_P} + \frac{\rho_N L_N}{S_N}\right) + R_{contact} \tag{13}$$

and

$$K = \left(\frac{\kappa_P S_P}{L_P} + \frac{\kappa_N S_N}{L_N}\right) \tag{14}$$

where $L$ and $S$ are, respectively, the leg length and cross-sectional area for the semiconductor arm, and $R_{contact}$ is the electrical resistance caused by the TEG junctions contact. Because the TEG is exoreversible, one has $T = T_H = T_1$ and $T_0 = T_C = T_2$ [57].

The output power of the TEG $P_{TEG}$ is given by [58]

$$P_{TEG} = \dot{Q}_H - \dot{Q}_C \tag{15}$$

Substituting Eqs. (11) and (12) into Eq. (15), $P_{TEG}$ can be further rewritten as

$$P_{TEG} = nI\left[\left(\alpha_1 T_1 - \alpha_2 T_2\right) - IR_g - \frac{\left(T_1 - T_2\right)\left(\tau_1 + \tau_2\right)}{2}\right] \tag{16}$$

The energetic efficiency $\eta_{TEG}$ of the TEG is given by [59]

$$\eta_{TEG} = \frac{P_{TEG}}{\dot{Q}_H} \tag{17}$$

Based on the second law of thermodynamics, the exergy destruction rate of the TEG $ExD_{TEG}$ can be expressed as

$$ExD_{TEG} = \dot{Q}_H\left(1 - \frac{T_0}{T}\right) - P_{TEG} \tag{18}$$

The exergetic efficiency of the TEG $\varphi_{TEG}$ is given by

$$\varphi_{TEG} = \frac{P_{TEG}}{\dot{Q}_H\left(1 - \frac{T_0}{T}\right)} \tag{19}$$

*2.4. Energetic and exergetic performances of the hybrid system*

The leaked heat rate from PAFC to the environment, $\dot{Q}_L$, can be described by [54]

$$\dot{Q}_L = K_L A_L (T - T_0) \tag{20}$$

where $K_L$ and $A_L$ are the heat-leak coefficient and heat-leak effective area of PAFC, respectively.

The rate of heat transferred to the TEG, $\dot{Q}_H$, is given by [60]

$$\dot{Q}_H = -\Delta \dot{H} - P_{FC} - \dot{Q}_L - \dot{Q}_{re} \tag{21}$$

Based on Eqs. (5), (20) and (21), $\dot{Q}_H$ can be further described by [44]

$$\dot{Q}_H = -\Delta \dot{H} - P_{PAFC} - \dot{Q}_L - \dot{Q}_{re} = A\left[ \left(1-\eta_{PAFC}\right) j \frac{-\Delta h}{n_e F} - \left(c_1 + c_2\right)\left(T - T_0\right) \right] \tag{22}$$

where $c_1 = [K_{re} A_{re} (1-\varepsilon)] / A$ and $c_2 = (K_L A_L) / A$ are two temperature-independent constants.

Equalizing Eqs. (11) and (22), the mathematical relationship between $j$ and $I$ can be analytically derived, i.e.,

$$n\left[ \alpha_1 I T_1 - \frac{I^2 R_g}{2} + K\left(T_1 - T_2\right) - \frac{\tau_1 I (T_1 - T_2)}{2} \right] = \frac{-A}{n_e F}\left[ \left(1-\eta_{FC}\right) j \Delta h - (c_1 + c_2)\left(T - T_0\right) \right] \tag{23}$$

According to the parameters in Table 2, the variations of $I$ with $j$ under different working temperature $T$ are shown in Fig. 2.

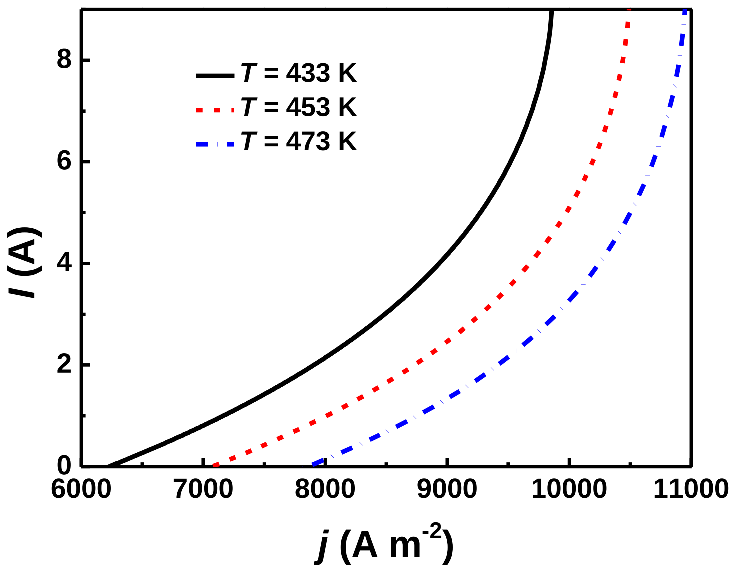


**Figure 2.** Curves of $I$ varying with $j$ under different $T$.

It is seen that $I$ increases with $j$, and the slope of $j$~$I$ is improved with the increasing $j$. The value of $j$ when the TEG begins to generate electric current rises with $T$. In addition, $I$ gradually decreases as $T$ increases.

**Table 2.** Equations used in the PAFC modeling [39, 50, 51].

| Parameter | Equation |
|---|---|
| Ideal standard potential | $E_0 = \frac{\Delta g^0}{n_e F}$ |
| Reversible voltage | $E_{rev} = \frac{\Delta g^0}{n_e F} + \frac{RT}{n_e F} \ln\left( p_{\mathrm{H_2}} p_{\mathrm{O_2}}^{0.5} / p_{\mathrm{H_2O}} \right)$ |
| Activation overpotential | $U_{act} = \frac{RT}{a n_e F} \ln\left( \frac{j}{j_0} \right)$ |
| Concentration overpotential | $U_{con} = b \exp(cj)$ |
| Ohmic overpotential | $U_{ohm} = j \frac{t_{ele}}{\sigma_{ele}}$ |
| Specific conductivity | $\sigma_{ele} = (\frac{702.7X^{1.5} - 1734.2X^2 + 1446.5X^{2.5} - 350.7X^3}{100\mu})$ $\exp[(-0.010163 + 0.011634X - 0.08313X^2)T]$ |
| Output voltage | $U = E_{rev} - U_{act} - U_{con} - U_{ohm}$ |

The power output $P$ and energetic efficiency $\eta$ for the PAFC-TEG hybrid system are, respectively, given by [27]

$$P = P_{FC} + P_{TEG} \tag{24}$$

and

$$\eta = \frac{P}{-\Delta \dot{H}} \tag{25}$$

The exergy destruction rate of the PAFC-TEG hybrid system, $ExD$, can be given by

$$ExD = -\Delta \dot{G} - \left( 1 - \frac{T_0}{T} \right) T \Delta \dot{S} - P \tag{26}$$

The exergetic efficiency of the PAFC-TEG hybrid system, $\varphi$, can be given by

$$\varphi = \frac{P}{-\Delta \dot{G} - \left( 1 - \frac{T_0}{T} \right) T \Delta \dot{S}} \tag{27}$$

## 3. GENERAL PERFORMANCE CHARACTERISTICS

The general performances for the PAFC-TEG hybrid system are illustrated in Fig. 3. It can be found from Fig. 3 that the TEG does not generate any electric power in the region of $j \le j_B$ or $j \ge j_M$. Therefore, the curves of $P^* \sim j$, $\eta \sim j$, $ExD^* \sim j$ and $\varphi \sim j$ respectively overlap with the curves of $P^*_{FC} \sim j$, $\eta_{FC} \sim j$, $ExD^*_{FC} \sim j$ and $\varphi_{FC} \sim j$ in the regions of $j \le j_B$ or $j \ge j_M$. Both $P^*$ and $P^*_{FC}$ first increase and then decrease with $j$ in its whole region, while $P^*_{TEG}$, $\eta_{TEG}$ and $\varphi_{TEG}$ have the same trend only in the region of $j_B < j < j_M$. Both $\eta$ and $\varphi$ firstly reduce then slightly increase and finally decrease with $j$, while $\eta_{FC}$ and $\varphi_{FC}$ monotonically decrease in the whole region of $j$. $ExD^*_{TEG}$ first decreases and then sharply increases as $j$ increases, while both $ExD^*$ and $ExD^*_{FC}$ monotonically increase in the whole region of $j$.

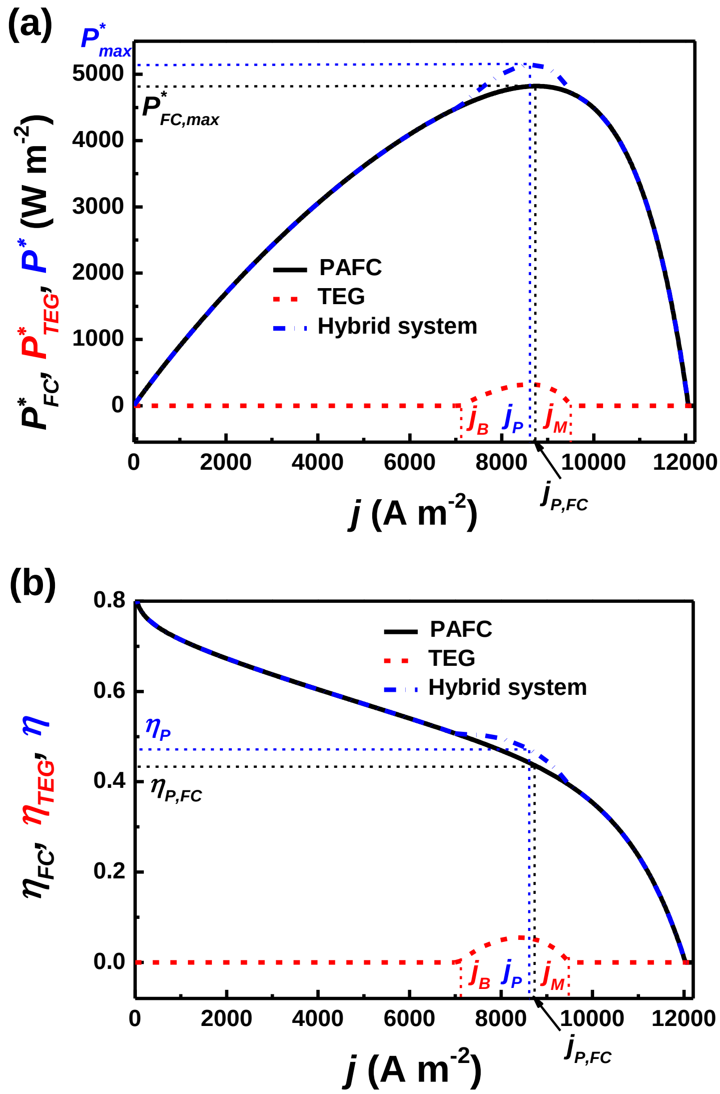

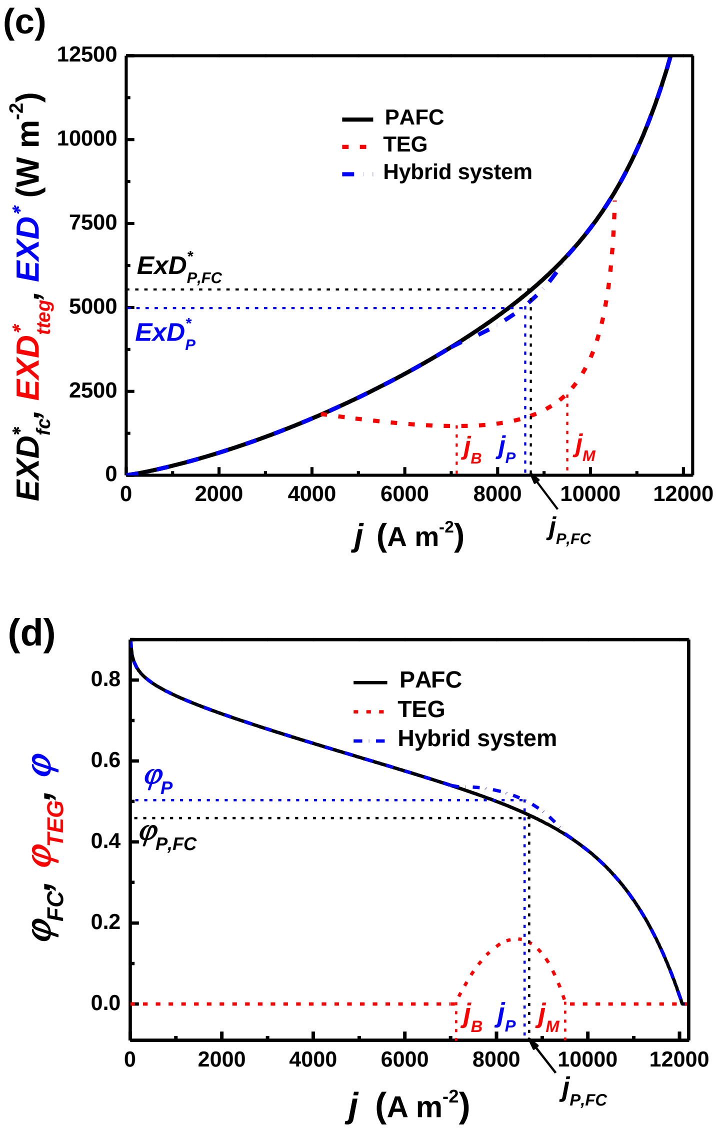


**Figure 3.** Energetic and exergetic performance comparisons of the PAFC, TEG and hybrid system for (a) output power densities, (b) energetic efficiencies, (c) exergy destruction rate densities, and (d) exergetic efficiencies; where $P^*_{FC} = P_{FC} / A$ ( $ExD^*_{FC} = ExD_{FC} / A$ ), $P^*_{TEG} = P_{TEG} / A$ ( $ExD^*_{TEG} = ExD_{TEG} / A$ ) and $P^* = P / A$ ( $ExD^* = ExD / A$ ) are, respectively, the power densities (exergy destruction rate densities) of PAFC, TEG and hybrid system; $P^*_{FC,\max}$ and $P^*_{max}$ are, respectively, the maximum output power densities of PAFC and PAFC-TEG system; $j_{P,FC}$ , $\eta_{P,FC}$ , $ExD^*_{P,FC}$ and $\varphi_{P,FC}$ are the current density, energetic efficiency, exergy destruction rate density and exergetic efficiency of PAFC when $P^*_{FC} = P^*_{FC,\max}$ ; $j_P$ , $\eta_P$ , $ExD^*_P$ and $\varphi_P$ are, respectively, the corresponding parameters of the hybrid system when $P^* = P^*_{\max}$ ; $j_B$ and $j_M$ are, respectively, the lower bound and upper bound for $j$ between which the TEG generates electric power, and its region span is $\Delta j = j_M - j_B$ .

**Table 3.** Designing and operating parameters used in the hybrid system modeling [5, 47, 50, 54].

| Parameter | Value |
|---|---|
| Faraday constant, $F$ (C mol$^{-1}$) | 96,485 |
| Universal gas constant, $R$ (J mol$^{-1}$ K$^{-1}$) | 8.314 |
| Number of electrons, $n_e$ | 2 |
| Operating pressure, $p$ (atm) | 1.0 |
| Operating temperature, $T$ (K) | 453 |
| Ambient temperature, $T_0$ (K) | 298 |
| Constant $b$ | 0.00003 |
| Constant $c$ | 0.0008 |
| Partial pressure of $H_2$, $p_{H_2}$ (atm) | 1.0 |
| Partial pressure of $O_2$, $p_{O_2}$ (atm) | 0.105 |
| Partial pressure of $H_2O$, $p_{H_2O}$ (atm) | 0.5 |
| Charge transfer coefficient, $a$ | 0.5 |
| Exchange current density, $j_0$ (A m$^{-2}$) | 0.06 |
| Thickness of the electrolyte, $t_{ele}$ (m) | 0.002 |
| Polar plate area of the cell, $A$ (m$^2$) | 0.0015 |
| Number of thermocouples, $n$ | 20 |
| Constant, $c_1$ (W K$^{-1}$ m$^{-2}$) | 0.1 |
| Constant, $c_2$ (W K$^{-1}$ m$^{-2}$) | 0.1 |

According to the typical parameters in Table 3, $P^*$ reaches its maximum $P^*_{\max}$, 5141.2 W m$^{-2}$, when $j = j_P = 8620.8$ A m$^{-2}$, while $P^*_{FC}$ attains its maximum $P^*_{FC,\max}$, 4822.4 W m$^{-2}$, when $j = j_{P,FC} = 8750.8$ A m$^{-2}$. $P^*_{\max}$ is approximately 6.6% higher than $P^*_{FC,\max}$. $\eta_P$ and $\eta_{P,FC}$ are, respectively, 47.1% and 43.7%, and $\eta_P$ is about 7.8% larger than $\eta_{P,FC}$. $\varphi_P$ and $\varphi_{P,FC}$ are, respectively, 50.1% and 46.5%, and $\varphi_P$ is about 7.7% larger than $\varphi_{P,FC}$. Meanwhile, $ExD_P^*$ and $ExD_{P,FC}^*$ are, respectively, 5120.7 W m$^{-2}$ and 5558.2 W m$^{-2}$, and $ExD_P^*$ is only 7.9% smaller than $ExD_{FC}^*$. From the above analyses, it is seen that the TEG is an effective way to utilize the exhaust heat from PAFC.

Adopting the maximum power density as an optimum criterion, the optimum range of $j$ for the PAFC-TEG hybrid system is given by [48]

$$j_B < j < j_P \tag{28}$$

The corresponding optimum regions of $P^*$, $\eta$, $ExD^*$ and $\varphi$ are, respectively, given by

$$P_B^* < P^* < P_{\max}^* \tag{29}$$

$$\eta_B > \eta > \eta_P \tag{30}$$

$$ExD_B^* < ExD^* < ExD_P^* \tag{31}$$

and

$$\varphi_B > \varphi > \varphi_P \tag{32}$$

where $P_B^*$, $\eta_B$, $ExD_B^*$ and $\varphi_B$ are the power density, energetic efficiency, exergy destruction rate density, exergetic efficiency of the hybrid system at $j_B$; $j_B$, $j_M$, $j_P$, $\Delta j$, $P_{\max}^*$, $\eta_P$, $\varphi_P$ and $ExD_P^*$ are eight vital parameters to evaluate the thermodynamic performances for the PAFC-TEG hybrid system.

**Table 4.** Vital performance parameters of PAFC-TEG hybrid system with and without Thomson effect.

| Thomson Effect | $j_B$ (A m$^{-2}$) | $j_M$ (A m$^{-2}$) | $\Delta j$ (A m$^{-2}$) | $j_P$ (A m$^{-2}$) | $P_{\max}^*$ (W m$^{-2}$) | $\eta_P$ (%) | $ExD_P^*$ (W m$^{-2}$) | $\varphi_P$ (%) |
|---|---|---|---|---|---|---|---|---|
| With | 7100.8 | 9510.8 | 2410.0 | 8620.8 | 5141.2 | 47.1 | 5120.7 | 50.1 |
| Without | 6510.8 | 9630.8 | 3120.0 | 8610.8 | 5315.3 | 49.0 | 4899.2 | 52.0 |

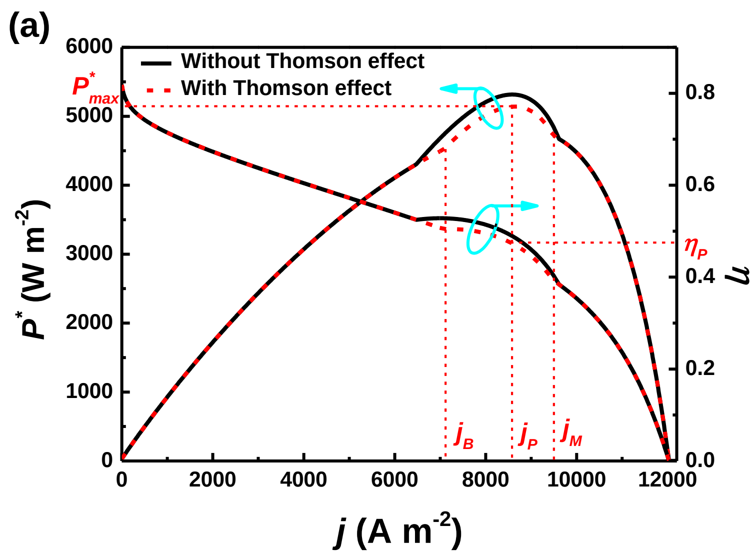

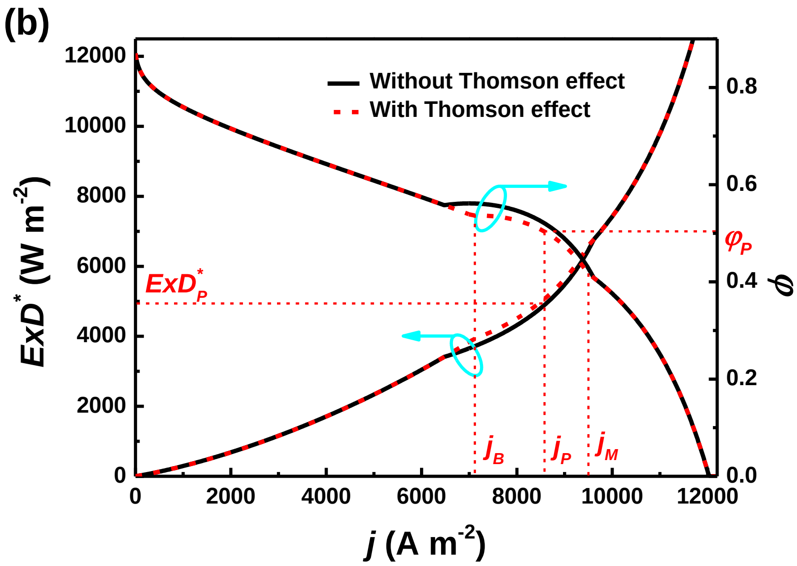


**Figure 4.** Influences of the Thomson effect on the hybrid system (a) energetic, and (b) exergetic performances.

The Thomson effect affecting the hybrid system performance is shown in Fig. 4, and the eight important performance parameters are listed in Table 4. It is found from Fig. 4 that $j_B$, $j_P$ and $ExD_P^*$ for the PAFC-TEG hybrid system considering the Thomson effect are greater than those ignoring the Thomson effect, while $j_M$ , $\Delta j$ , $P^*_{\max}$ , $\eta_P$ and $\varphi_P$ of the PAFC-TEG hybrid system considering the Thomson effect are less than those ignoring the Thomson effect. Although the Thomson effect deteriorates the thermodynamic performances for the hybrid system, the results considering the Thomson effect are closer to the actual situations.

In comparison with the PAFC/TEG-TEC hybrid system model in Ref. [49], the present model performs better because a large exergy destruction occurs in the TEC cooling processes. In addition, the present model also performs better than the PAFC/absorption refrigerator hybrid system model in Ref. [51] although the effective operating current density region of the latter is larger than the present model.

## 4. PARAMETRIC STUDIES

Based on the above equations, the hybrid system energetic and exergetic performances depend on some operating conditions and designing parameters, such as working temperature ( $T$ ), phosphoric acid concentration ($X$), exchange current density ( $j_0$ ) and thermocouple number ( $n$ ). These vital parameters listed in Table 3 will be considered as default ones in the following analysis unless specifically mentioned.

### *4.1. Effect of the operating temperature ( $T$ )*

Although a higher working temperature of PAFC leads to bigger thermodynamic losses as shown in Eq. (4), it is always preferable for the whole hybrid system performance as shown in Fig. 5. This can be interpreted that the performance improvements of PAFC and TEG are bigger than the performance suppression resulting from the thermodynamic losses. By increasing the operating temperature $T$, $P^*$, $\eta$ and $\varphi$ are improved in the whole regions of $j$, while $ExD^*$ is reduced.

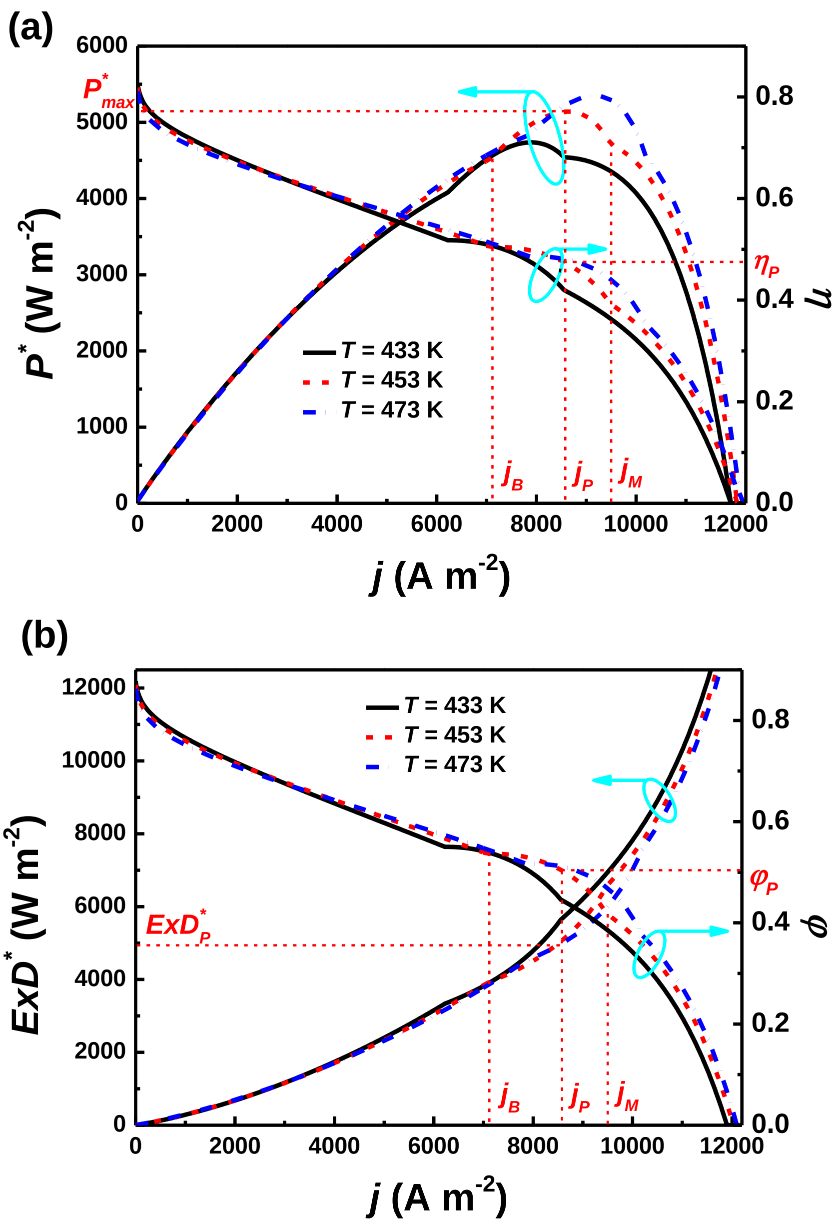


**Figure 5.** Influences of $T$ on the hybrid system (a) energetic, and (b) exergetic performances.

**Table 5.** Vital performance parameters of the hybrid system under different $T$.

| $T$ (K) | $j_B$ (A m$^{-2}$) | $j_M$ (A m$^{-2}$) | $\Delta j$ (A m$^{-2}$) | $j_P$ (A m$^{-2}$) | $P^*_{\max}$ (W m$^{-2}$) | $\eta_P$ (%) | $ExD^*_P$ (W m$^{-2}$) | $\varphi_P$ (%) |
|---|---|---|---|---|---|---|---|---|

| | | | | | | | | |
|---|---|---|---|---|---|---|---|---|
| 433 | 6220.8 | 8590.8 | 2370.0 | 7890.8 | 4736.4 | 47.4 | 4657.0 | 50.4 |
| 453 | 7100.8 | 9510.8 | 2410.0 | 8620.8 | 5141.2 | 47.1 | 5120.7 | 50.1 |
| 473 | 7780.8 | 10260.8 | 2480.0 | 9170.8 | 5349.38 | 46.1 | 5568.2 | 49.0 |

Table 5 further shows that $j_B$, $j_M$ , $j_P$, $P^*_{\max}$ , $ExD^*_P$ are improved as $T$ increases from 433 to 473 K. $\eta_P$ and $\varphi_P$ slightly decrease, while $\Delta j$ first increases and then decreases as $T$ increases from 433 K to 473 K.

*4.2 Effect of the exchange current density ( $j_0$)*

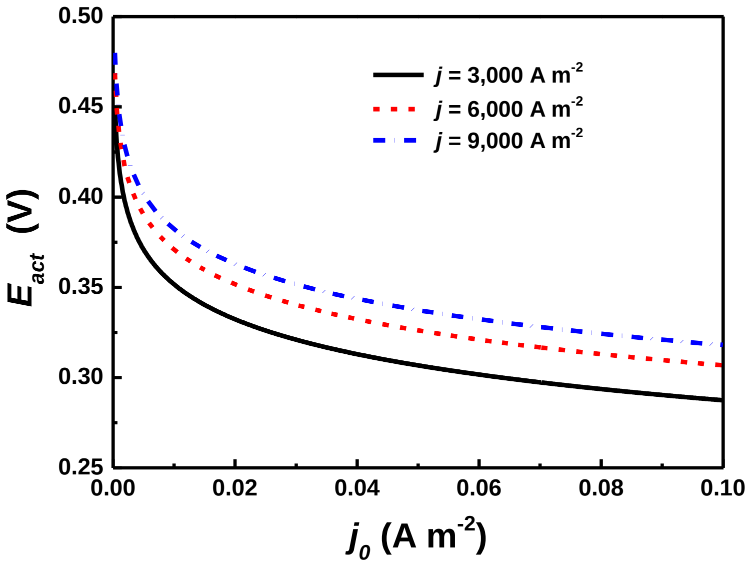


**Figure 6.** Influences of $j_0$ on $E_{act}$ .

**Table 6.** Vital performance parameters of the hybrid system under different $j_0$ .

| $j_0$ ( A m$^{-2}$) | $j_B$ (A m$^{-2}$) | $j_M$ (A m$^{-2}$) | $\Delta j$ (A m$^{-2}$) | $j_P$ (A m$^{-2}$) | $P^*_{\max}$ (W m$^{-2}$) | $\eta_P$ (%) | $ExD^*_P$ (W m$^{-2}$) | $\varphi_P$ (%) |
|---|---|---|---|---|---|---|---|---|
| 0.02 | 6880.8 | 9330.8 | 2450.0 | 8470.8 | 4870.5 | 45.6 | 5178.0 | 48.5 |
| 0.06 | 7100.8 | 9510.8 | 2410.0 | 8620.8 | 5141.2 | 47.1 | 5120.7 | 50.1 |
| 0.1 | 7210.8 | 9600.8 | 2390.0 | 8730.8 | 5267.6 | 47.8 | 5089.3 | 50.2 |

The exchange current density of PAFC $j_0$ is a significant parameter that impacts the activation overpotential of the PAFC $E_{act}$. As shown in Fig. 6, $E_{act}$ increases as $j$ increases from 3000 to 9000 A $m^{-2}$. $E_{act}$ decreases as $j_0$ increases, and the slope of $j_0 \sim E_{act}$ is improved with $j_0$.

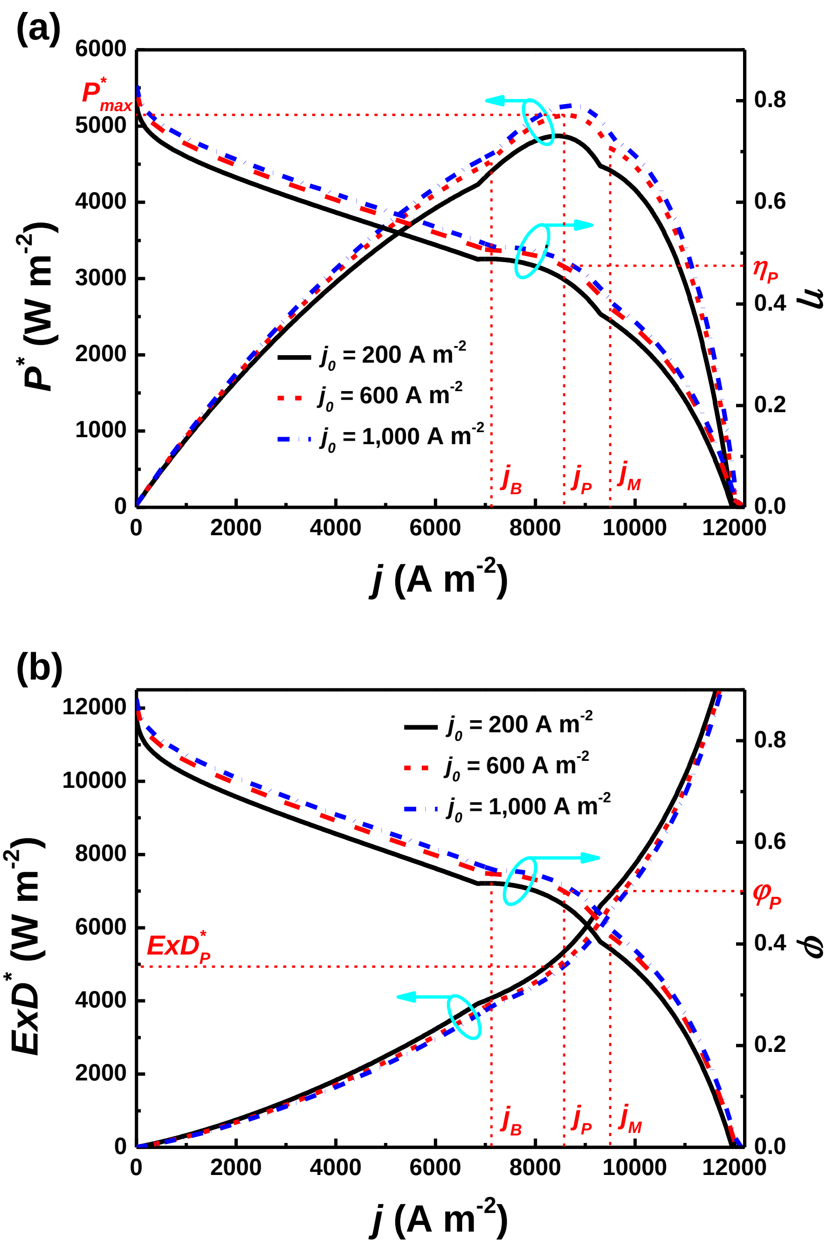


**Figure 7.** Influences of $j_0$ on the hybrid system (a) energetic, and (b) exergetic performances.

Thus, a larger $j_0$ is always beneficial for the PAFC-TEG hybrid system performance, as shown in Fig. 7. With the increasing of $j_0$, $P^*$, $\eta$ and $\varphi$ are improved while $ExD^*$ is reduced in the whole region of $j$. As listed in Table 6, $j_B$, $j_M$, $j_P$, $P^*_{\max}$, $\eta_P$, $ExD^*_P$ and $\varphi_P$ are improved, while $\Delta j$, $\eta_P$ and $\varphi_P$ are decreased when $j_0$ grows from 0.02 to 0.1 A $m^{-2}$.

*4.3. Effect of the phosphoric acid concentration ( $X$ )*

**Table 7.** Vital performance parameters of the hybrid system under different $X$ .

| $X$ (%) | $j_B$ (A m$^{-2}$) | $j_M$ (A m$^{-2}$) | $\Delta j$ (A m$^{-2}$) | $j_P$ (A m$^{-2}$) | $P^*_{\max}$ (W m$^{-2}$) | $\eta_P$ (%) | $ExD^*_P$ (W m$^{-2}$) | $\varphi_P$ (%) |
|---|---|---|---|---|---|---|---|---|
| 92.5 | 7310.8 | 9730.8 | 2420.0 | 8880.0 | 5432.4 | 48.5 | 5102.4 | 51.6 |
| 97.5 | 7100.8 | 9510.8 | 2410.0 | 8620.8 | 5141.2 | 47.1 | 5120.7 | 50.1 |
| 100 | 7060.8 | 9460.8 | 2400.0 | 8600.8 | 5071.6 | 46.8 | 5131.0 | 49.7 |

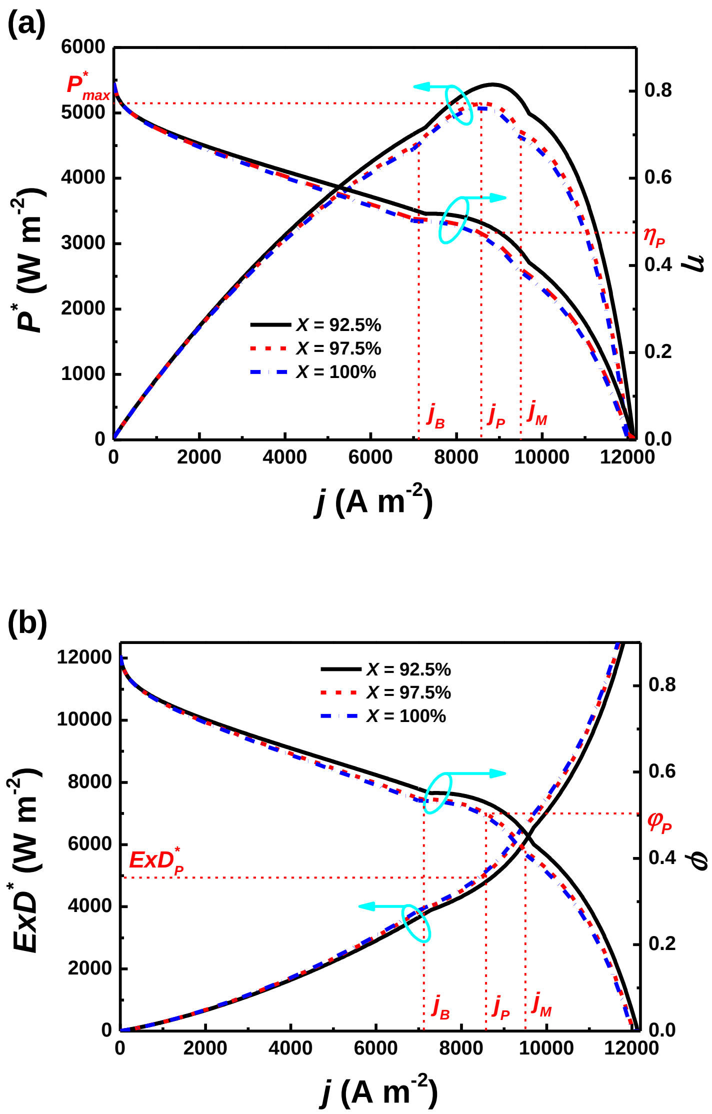


**Figure 8.** Influences of $X$ on the hybrid system (a) energetic, and (b) exergetic performances.

$\chi$ is the phosphoric acid concentration of the electrolyte, which dramatically affects the ohmic overpotential of PAFC $E_{ohm}$, and therefore, it plays a significant role in the PAFC output voltage degradation.

This is because the amount of conductive ions and the interaction between ions will be improved with an increase in $\chi$, while the mobility of conductive ions is degraded with the increasing $\chi$. Therefore, the specific ionic conductivity is decreased and the ohmic overpotential is increased. As a result, the growth of $\chi$ degrades the hybrid system performance, as shown in Fig. 8. $P^*$, $\eta$ and $\varphi$ decrease while $ExD^*$ increases with $\chi$ in the whole region of $j$. As illustrated in Table 7, $ExD_P^*$ increases while $j_B$, $j_M$, $\Delta j$, $j_P$, $P_{\max}^*$, $\eta_P$ and $\varphi_P$ decrease as $\chi$ increases.

*4.4. Effect of the thermocouple number ($n$)*

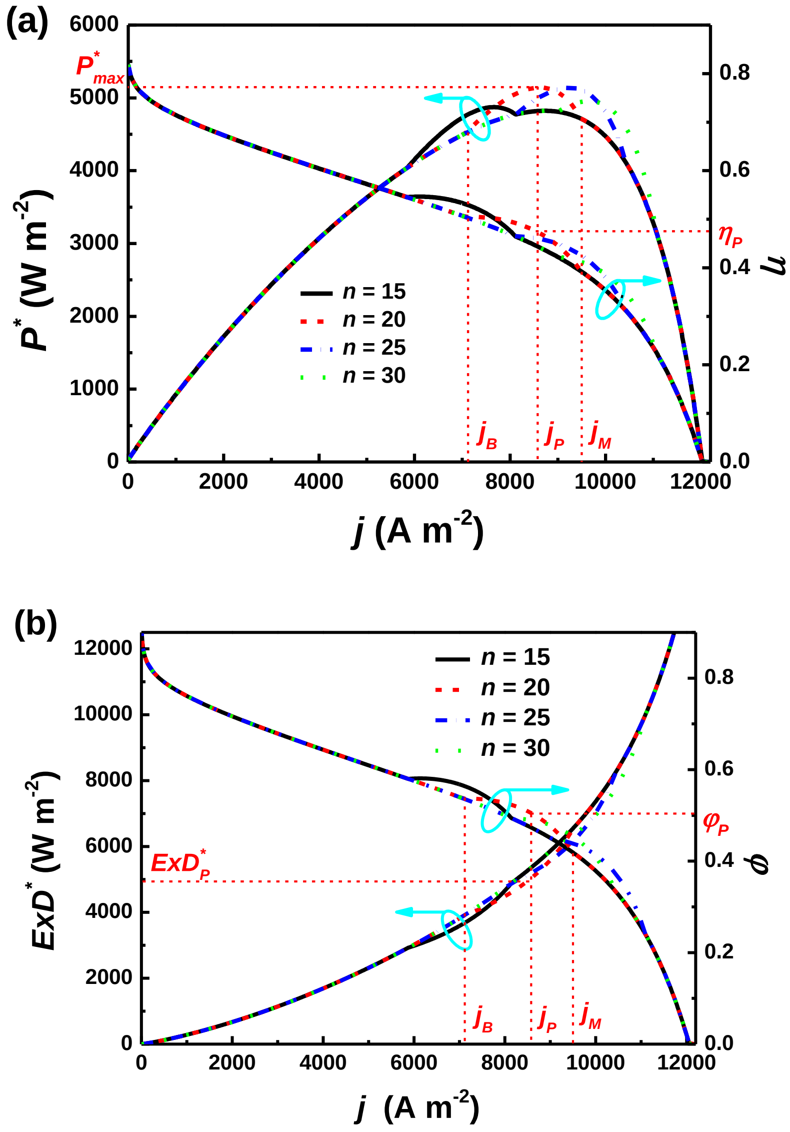


**Figure 9.** Influences of $n$ on the hybrid system (a) energetic, and (b) exergetic performances.

A bigger $n$ implies that more thermocouples are used in this hybrid system, which is conductive to improve the TEG performance as well as the hybrid system performance. As illustrated in Fig. 9, the effect of thermocouple number only occurs in the region of $j_B < j < j_M$. A larger $n$ makes the TEG working range ( $j_B < j < j_M$ ) move rightward.

**Table 8.** Vital performance parameters of the hybrid system under different $n$ .

| $n$ (-) | $j_B$ (A m$^{-2}$) | $j_M$ (A m$^{-2}$) | $\Delta j$ (A m$^{-2}$) | $j_P$ (A m$^{-2}$) | $P^*_{\max}$ (W m$^{-2}$) | $\eta_P$ (%) | $ExD^*_P$ (W m$^{-2}$) | $\varphi_P$ (%) |
|---|---|---|---|---|---|---|---|---|
| 15 | 5880.8 | 8150.8 | 2270.0 | 7690.8 | 4872.6 | 50.2 | 4250.5 | 53.4 |
| 20 | 7100.8 | 9510.8 | 2410.0 | 8620.8 | 5141.2 | 47.1 | 5120.7 | 50.1 |
| 25 | 8160.8 | 10460.8 | 2300.0 | 9280.8 | 5139.2 | 43.9 | 5870.1 | 46.7 |
| 30 | 9030.8 | 11100.8 | 1970.0 | 9680.8 | 4956.7 | 40.6 | 6527.1 | 43.2 |

As shown in Table 7, $j_B$ , $j_M$ , $j_P$ and $ExD^*_P$ increase while $\eta_P$ and $\varphi_P$ decrease as $n$ increases from 15 to 30. It is also noticed that both $P^*_{\max}$ and $\Delta j$ increase at first and then decrease as $n$ increases. Based on the calculation examples in Table 8, the optimum value of $n$ is found to be between 20~25.

## 5. CONCLUSIONS

In order to accurately evaluate the potential of TEG to utilize PAFC waste heat, the theoretical model for a PAFC-TEG hybrid system with the Thomson effect is proposed. Through systematic analysis of multiple irreversible losses in PAFC-TEG hybrid system, the energy and exergy mathematical expressions for the proposed system are obtained. The relationship of the PAFC working current density with respect to the TEG electric current is derived. Calculations show that the proposed system is feasible and more effective than a stand-alone PAFC system. The maximum power output density and the corresponding energetic efficiency and exergetic efficiency for the PAFC-TEG hybrid system permit 6.6%, 7.8% and 7.7% greater than that of a single PAFC system, respectively. Meanwhile, the exergy destruction rate density is decreased by 7.8%. The optimum operating regions and the impacts of the Thomson effect on the hybrid system performance are obtained. The impacts of some important designing parameters and operation conditions on the hybrid system performances are systematically analyzed. The results obtained in this article may be helpful for the performance improvement of a PAFC system by utilizing cogeneration technologies.

ACKNOWLEDGMENTS
This work has been supported by the Natural Science Foundation of Zhejiang Province (Grant No. LY20E060002), and the K. C. Wong Magna Fund in Ningbo University, China.

**References**

1. N.L. Panwar, S.C. Kaushik and S. Kothari, *Renew. Sust. Energ. Rev.*, 15 (2011) 1513.
2. Z. Wu, P. Zhu, J. Yao, P. Tan, H. Xu, B. Chen, F. Yang, Z. Zhang and M. Ni, *Energy*, 192 (2020) 116613.
3. M. Mehrpooya, P. Bahramian, F. Pourfayaz and M.A Rosen, *Sustain. Energy Technol. Assess.*, 18 (2016) 100.
4. W. Hu, W. Chen and H. Wang, *Int. J. Electrochem. Sci.*, 14 (2019) 3229.
5. H.S. Wang, C.P. Chang, Y.J. Huang, Y.C. Su and F.G. Tseng, *Energy*, 133 (2017) 1142.
6. C.L. Lu, C.P. Chang, Y.H. Guo, T.K. Yeh, Y.C. Su, P.C. Wang, H.L. Hsueh and F.G. Tseng, *Renew. Energy*, 134 (2019) 982.
7. G.F. McLean, T. Niet, S. Prince-Richard and N. Djilali, *Int. J. Hydrogen Energy*, 27 (2002) 507.
8. J. Fang, M. Lyu, X. Wang, Y. Wu and J. Zhao, *J. Power Sources*, 284 (2015) 517.
9. O. Muneeb, E. Do, D. Boyd, J. Perez and J.L. Haan, *Appl. Energy*, 235 (2019) 473.
10. T.V. Nguyen and R.E. White, *J. Electrochem. Soc.*, 140 (1993) 2178.
11. P. Chandran and S. Ramaprabhu, *Int. J. Hydrogen Energy*, 43 (2018) 18477.
12. Z. Li, R. Outbib, S. Giurgea and D. Hissel, *IEEE Trans. Energy Convers.*, 34 (2019) 3.
13. Y. Tian, Z. Lü, X. Guo and P. Wu, *Int. J. Electrochem. Sci.*, 14 (2019) 1093.
14. L. Chen, S. Gao and H. Zhang, *Int. J. Electrochem. Sci.*, 8 (2013) 10772.
15. S. Wang and S.P. Jiang, *Natl. Sci. Rev.*, 4 (2017) 163.
16. P.L. Zervas, M.K. Koukou and N.C. Markatos, *Energ. Convers. Managem.*, 47 (2006) 2883.
17. S.R. Choudhury, S.R. Choudhury, J. Rangarajan and R. Rengaswamy, *J. Power Sources*, 140 (2005) 274.
18. R. Lan, X. Xu, S. Tao and J.T.S. Irvine, *J. Power Sources*, 195 (2010) 6983.
19. T.T. Aindow, A.T. Haug and D. Jayne, *J. Power Sources*, 196 (2011) 4506.
20. H.Y. Kwak, H.S. Lee, J.Y. Jung , J.S. Jeon and D.R. Park, *Fuel*, 83 (2004) 2087.
21. R.K. Pachauri and Y.K. Chauhan, *Int. J. Elec. Power*, 74 (2016) 49.
22. Y. Zhao, C. Ou and J. Chen, *Int. J. Hydrogen Energy*, 33 (2018) 4161.
23. H. Zhang, L Chen, J. Zhang and J. Chen, *Energy*, 68 (2014) 1.
24. M. Ishizaw, S. Okada and T. Yamashita, *J. Power Sources*, 86 (2000) 294.
25. E. Açıkkalp and M.H. Ahmadi, *J. Clean. Prod.*, 203 (2018) 585.
26. X. Chen, Y. Wang, L. Cai and Y. Zhou, *J. Power Sources*, 294 (2015) 430.
27. E. Açıkkalp, *J. Therm. Eng.*, 5 (2019) 29.
28. M. Marefati and M. Mehrpooya, *Sustain. Energy Technol. Assess.*, 36 (2019) 100550.
29. W. He, G. Zhang, X. Zhang, J. Ji, G. Li and X. Zhao, *Appl. Energy*, 143 (2015) 1.
30. X. Gou, H. Xiao and S. Yang, Appl. *Energy*, 87 (2010) 3131.
31. L. Merotto, L.C. Fanciulli, R. Dondè and S.D. Iuliis, *Appl. Energy*, 162 (2016) 346.
32. X. Gou, S. Yang, H. Xiao and Q. Ou, *Energy*, 52 (2013) 201.
33. S. Wu, H. Zhang and M. Ni, *Energy*, 112 (2016) 520.
34. X. Gao, S.J. Andreasen, S.K. Kær and L.A. Rosendahl, *Int. J. Hydrogen Energy*, 39 (2014) 6637.
35. X. Gao, S.J. Andreasen, M. Chen and S.K. Kær, *Int. J. Hydrogen Energy*, 37 (2012) 8490.
36. M. Chen, S.J. Andreasen, L. Rosendahl, S.K. Kær and T. Condra, *J. Electron. Mater.*, 39 (2010) 1593.

37. P. Yang, Y. Zhu, P. Zhang, H. Zhang, Z. Hu and J. Zhang, *Int. J. Hydrogen Energy*, 39 (2014) 11756.
38. J. Liu, H. Zhang, J. Wang, J. Zhao, F. Wang, H. Miao, J. Yuan and S. Hou, *Int. J. Electrochem. Sci.*, 14 (2019) 3701.
39. X. Chen, Y. Pan and J. Chen, *Fuel Cells*, 10 (2010) 1164.
40. L.A. Rosendahl, P.V. Mortensen and A.A. Enkeshafi, *J. Electron. Mater.*, 40 (2011) 1111.
41. J. Chen, Z. Yan and L. Wu, J. *Appl. Phys.*, 79 (1996) 8823.
42. S. Manikandan and S.C. Kaushik, *Sol. Energy* 135 (2016) 569.
43. Y. Feng, L. Chen, F. Meng and F. Sun, *Entropy*, 20 (2018) 29.
44. H. Zhang, W. Kong, F. Dong, H. Xu, B. Chen and M. Ni, *Energ. Convers. Managem.*, 148 (2017) 1382.
45. S.C. Kaushik and S. Manikandan, E*nerg. Convers. Managem.*, 103 (2015)200-7.
46. R. Lamba and S.C. Kaushik, *Energ. Convers. Managem.*, 144 (2017) 388.
47. S. Manikandan and S.C. Kaushi, *Energy*, 100 (2016) 227.
48. H. Zhang, G. Lin and J. Chen, *Int. J. Hydrogen Energy*, 37 (2012) 3438 .
49. M. Wu, H. Zhang, J. Zhao, F. Wang and J. Yuan, *Int. J. Refrig.*, 89 (2018) 61.
50. X. Chen, Y. Wang, Y. Zhao and Y. Zhou, *Energy*, 101 (2016) 359.
51. P. Yang, H. Zhang and Z. Hu, I*nt. J. Hydrogen Energy*, 41 (2016) 3579.
52. F. Meng, L. Chen, Y. Feng and B. Xiong, *Energy*, 135 (2017) 83.
53. M. Kalteh and H. Akhlaghi Garmejani, *Int. J. Green Energy*, 16 (2019) 917.
54. E. Açıkkalp, *Energ. Convers. Managem.*, 148 (2016) 279.
55. R. Arora and R. Arora, *J. Renew. Sustain.,* 10 (2018) 044701.
56. C. Fuqiang, H. Yanji and Z. Cha, J. *Energy Resour. Technol.*, 136 (2014) 011201.
57. Y. Feng, L. Chen, F. Meng and F. Sun, *J. Non-Equilib. Thermodyn.*, 43 (2018) 75.
58. S. Qing, A. Rezania, L.A. R osendahl and X. Gou, *Ieee Access*, 6 (2018) 60852.
59. G. Özel, E. Açkkalp, A.F. Sava and H. Yamk, J. *Non-Equilib. Thermodyn.*, 41 (2016) 225.
60. M. Zhao, H. Zhang, Z. Hu, Z. Zhang and J. Zhang, *Energ. Convers. Managem.*, 89 (2015) 683.